A gentle approach to investigate the influence of LRP-1 silencing on the migratory behavior of breast cancer cells by atomic force microscopy and dynamic cell studies.

A Berquand, M Meunier, O Campion, S Dedieu, M Molinari, Jt Devy

A gentle approach to investigate the influence of LRP-1 silencing on the migratory behavior of breast cancer cells by Atomic Force Microscopy and dynamic cell studies

Alexandre Berquand[1], PhD, Marie Meunier[2], MS, Jessica Thevenard Devy[2], PhD, Corinne Ivaldi[2], PhD, Océane Campion[2], MS, Stéphane Dedieu[2], PhD, Michael Molinari[1,3]*, PhD, Jérôme Devy PhD[2]*

[1] Laboratoire de Recherche en Nanosciences LRN EA4682 and NanoMat' platform, Université de Reims Champagne-Ardenne, F-51685 Reims, FR

[2] CNRS UMR 7369: Matrice Extracellulaire et Dynamique Cellulaire (MEDyC), UFR Sciences Exactes et Naturelles, Université de Reims Champagne-Ardenne (URCA), Laboratoire SiRMa - Campus Moulin de la Housse, BP 1039, 51687, Reims cedex, FR

[3] CNRS UMR 5248: Matrice Extracellulaire et Dynamique Institute of Chemistry and Biology of Membranes and Nanoobjects (CBMN), INP Bordeaux, Université de Bordeaux, 33600 Pessac, FR

* Author for correspondence: jerome.devy@univ-reims.fr, (phone 33 326 91 32 82),
michael.molinari@u-bordeaux.fr (phone 33 326 05 19 01)

Authors disclosed no potential conflicts of interest

The authors thank the Region Champagne Ardenne, URCA and CNRS.

Word count for abstract: 142 words
Complete manuscript word count: 5000 words
Number of references: 58
Number of figures: 8
Number of tables: 1
Number of Supplementary online-only files: 3 (2 movies, 1 supplementary information and figure legend)

Abstract

To get more insight into the role of LRP-1 in the mechanism of tumor progression in triple negative breast cancer. Atomic force microscopy, videomicroscopy, confocal microscopy and Rho-GTPAse activity assay were used on MDA-MB-231 and LRP-1-silenced cells. Silencing of LRP-1 in MDA-MB-231 cells was shown to led to a dramatic increase in the Young's modulus in parallel to a spectacular drop in membrane extension dynamics as well as a decrease in the cells migration abilities on both collagen I and fibronectin substrates. These results were perfectly correlated to a corresponding change in cell morphology and spreading capacity as well as in Rho-GTPases activity. By a multi-technique approach, it was demonstrated that LRP-1 played a crucial role in the migration of MDA-MB-231 cells by modulating the membrane extension dynamic. The originality of this AFM investigation lies in the non-invasive aspect of the measurements.

Keywords: LRP-1 °Triple Negative Breast Cancer ° Atomic Force Microscopy

Background

The low-density lipoprotein receptor-related protein-1 (LRP-1) is a large multifunctional endocytic receptor involved in the clearance of various molecules from the extracellular matrix. LRP-1 is synthesized as a 600 kDa precursor and maturated in a 515 kDa α-chain noncovalently linked to a 85 kDa transmembrane and intracellular β-chain. The extracellular α-chain protruding in the extracellular space is composed of four interaction domains of ligand-binding type cystein-rich repeats able to bind more than forty ligands as lipoproteins, extracellular matrix (ECM) macromolecules, proteinases, proteinase/inhibitor complexes [1, 2]. The LRP-1 β chain includes YxxL, a dileucine and two NPxY motifs involved in endocytosis and as binding sites for signaling adapter proteins. LRP-1 is involved in many physiological and pathological processes including the regulation of vascular integrity [3], blood brain barrier permeability [4], peripheral nerve regeneration [5], or in the cell migration and proliferation [6].

Over the last decade, many studies have also highlighted the role of LRP-1 in the regulation of proteolytic cascades involved in tumor progression, although this was subject to controversy. Indeed, LRP-1 was reported to exhibit anti-tumor properties in cell lines derived from prostate [7], kidney [8], colon [9, 10] or endometrium [11] cancers, and pro-tumor properties in cell lines derived from brain cancer [12]. Interestingly, LRP-1 was also found to drive both anti-and pro-tumor functions in the same cell line, like shown for those derived from thyroid [13, 14] and breast [7, 15, 16] cancers. As shown in previous studies conducted from thyroid carcinomas, the pro-tumor role of LRP-1 mainly lies in its capacity to control the cytoskeleton organization. Particularly, LRP-1 balances the traction and adherence forces and rules the internalization of adherence complexes [14, 17]. Therefore, there is a critical

need to identify the precise role of this endocytic receptor during tumor progression and to decipher the underlying mechanisms.

Various studies have prompted the importance of heterogeneity in cell mechanical properties on adhesion, division and migration capabilities. The easiest way to appraise such properties is to assess the cell stiffness. Among the most commonly used techniques, one can cite micropipette aspiration [18], microfluidics [19], optical trapping [20], magnetic tweezers [21], traction force microscopy [22], and atomic force microscopy [23-26]. This last technique developed in the 80's [27] turned out to be one of the most proper technique to assess the topography and the mechanical properties of live cells in near-physiological conditions [28, 29].

Over the last 15 years, numerous studies reported that cancer cells and their normal counterparts exhibited different mechanical properties. Generally speaking, in response to an indenter-mediated stimulation, cancer cells are softer than their homologues. This has been proved in the case of bladder [30], blood [31], breast [32] and others tissues. The pioneering experiment of AFM imaging on live cells was performed in 1992 [33] where the dynamic behavior of the cytoskeleton of glial cells was investigated in contact mode. In 90's, tapping mode [34] was released to avoid this drawback; in that case, the tip only intermittently interacts with the surface, resulting in negligible friction and shear forces. Nevertheless, with both techniques, extracting the sample's mechanical properties is not possible. On the contrary, force spectroscopy, and more in particular, force volume can be used to map the stiffness and the adhesion of live cells in a quantitative manner [35, 36], although the technique suffers from a very slow acquisition speed. To overcome this limitation, the PeakForce QNM technique, an oscillating mode where loading forces can be minimized and from which quantitative mechanical information can be obtained in a

reasonable amount of time, has been developed. This technique has been already successfully used to image and investigate the mechanical properties of live U-251 cancer cells [37].

In a previous work [38], standard force spectroscopy was used to extract the average Young's modulus of FTC-133 cells using colloidal probes but due to the slow acquisition speed, it was not possible to follow the dynamics of the cell properties in real-time and to correlate the results with the migration properties of the studied cells while it seems important to clearly understand the role of LRP-1. In the present study, the PeakForce QNM mode was used to probe the differences between control cells (shCtrl) and LRP-1 silenced breast cancer live cells (shLRP-1) in terms of topography, mechanical properties and migration abilities on collagen I and fibronectin substrates, in parallel to videomicroscopy, confocal and RHoGTPases activity experiments.

Methods

Cell Culture

All the experiments were performed using a human breast cancer adenocarcinoma cell line (MDA-MB-231) provided by the American Type Culture Collection (ATCC, catalogue No. ATCC- HTB-26™). The cells were grown in Dulbecco's Modified Eagle Medium (DMEM) supplemented with GlutaMAX™-I (PAN-Biotech) and 10% fetal bovine serum (FBS; PAN-Biotech) at 37°C in a 5% CO2 atmosphere. LRP-1 silencing in MDA-MB-231 cells was achieved using a LacSwitch II mammalian expression system (Agilent Technologies, Stratagene Products Division, La Jolla, USA) and shRNA sequences described by Dedieu et al [14].

Fibronectin and type I collagen coating

The fibronectin used for all experiments came from bovine plasma (Sigma-Aldrich, Saint-Louis, USA). The fibronectin [1mg/ml] was diluted with sterile PBS solution to a final concentration of 7µg/ml. The type I collagen was purchased from Stago (Stago BNL, Netherlands), diluted according to the specifications of the supplier, and used at a concentration of 35µg/ml. A saturation step with 1% denatured BSA has been done before seeding the cells.

RT-qPCR and western blot analysis

Briefly, a mass of up to 250 ng of the isolated RNAs was used for cDNA synthesis. The mixtures were incubated in a thermocycler at 42 °C for 30 min and 95 °C for 2 min. Realtime PCR conditions were 15 min at 95 °C followed by 40 cycles of 15 s at 95 °C (denaturation) and 1 min at 60 °C (annealing/extension). MDA-MB-231 shCTRL was chosen to represent a 1× expression of the genes of interest, and the levels in the treated samples were expressed relatively to those in the corresponding control sample. For western blotting, the cells lysates were harvested and centrifuged. The proteins were separated by electrophoresis and transferred onto a nitrocellulose membrane. The membranes were incubated in blocking buffer for 1 h at room temperature and incubated overnight at 4 °C with an anti-LRP-1 primary antibody (EPR3724, abcam, Paris, France) in blocking buffer. After washes, the membranes were incubated in the presence of a secondary antibody, and after revelation the bands from the immunoblots were quantified.

Immunofluorescence

Cells (25×10^4) were plated on glass-slides, coated with fibronectin or type I collagen and incubated for 24h `at 37°C. The fixation of the samples was made using 4% (v/v) paraformaldehyde. The slides were washed with PBS, incubated with BSA 3% (w/v) for 30 min and overnight with an anti-talin antibody (Merck millipore, Fontenay sous bois, France).

Then cells were washed with PBS and incubated for 45 min with an Alexafluor-488-conjugated phalloidin and with an anti-rabbit Alexfluor-568 (Thermofisher, Villebon sur Yvette, France). . Slides were incubated with mounting medium containing DAPI. Immunofluorescence-labeled cell preparations were analyzed using a Zeiss LSM 710 confocal laser scanning microscope with the 63X oil-immersion objective Zeiss operating system (Carl Zeiss MicroImaging GmbH, Deutschland). Projection and surfacic representations were realized using AMIRA (v6.2) software (Thermofisher, Villebon sur Yvette, France). To compare cell labeling, a same threshold was applied for each channel of shCtrl *versus* shLRP-1 cells. For colocalization studies, a multichannel field module was used, followed by a correlation plot treatment (sub-ranges values 15–255, gamma 0.5).

AFM imaging

A Bioscope Catalyst^{TM} (Bruker, Billerica, USA) coupled to a Nikon Eclipse Ti inverted microscope (Nikon, Tokyo, Japan) were used for the AFM experiments. PFQNM mode was systematically used to obtain mapping of the Young's modulus as it allows a higher resolution at faster acquisition speed than the classical Force-Volume measurements [39]. Preliminary experiments in force-volume (see supplementary information) mode were also performed for each cell type and have shown that the two modes give similar results for the Young's modulus values as already shown by other comparative studies using nanomechanical modes [40].

PFQNM-LC-A-CAL probes, having a nominal spring constant of 0.1 N/m and a resonance frequency of ~45 kHz were used to image the cells, the tips being calibrated as previously described [41]. The tip geometry ("ace of spades" pyramidal shape, with a tip height of 17 µm and an apex diameter of 130 nm) was designed on purpose to minimize the background effect. For PFQNM experiments, we used a PeakForce frequency of 0.25 kHz so to be as low

as possible in order to maximize the contact time between the tip and the sample, a PeakForce amplitude of 1 µm so to be as high as possible since the cells are quite high.

Images were captured in culture medium at a resolution of 256 or 128 pixels per line, at 37°C using a Perfusing Stage Incubator (Bruker, Billerica, USA). The petri dish was put on the baseplate when the temperature setpoint was reached and stable over time. The Young's modulus, step height, surface and volume measurements were calculated using Nanoscope Analysis (Bruker, Billerica, USA). Regarding the Young's modulus calculation, for each type of cells, 3 different cell dishes coming from the same culture were analyzed one after the other to avoid to work more than 3 hours with each dish and the experiments were triplicated to draw a reliable conclusion. At the end, between 45 and 60 cells for each condition. Referring to both the information displayed by the deformation channel and the cross section on the height channel, the measurements were made only at locations were the cell height was at least 4 times superior to the indentation depth, i.e. in cell area with a minimum height of 1µm, in order to exclude any influence of the substrate on the measured values. Thus, perinuclar areas were avoided. The Sneddon approximation [42] was used to estimate the interaction between the tip and the substrate. In order to avoid generating mechanical stress to the cells, the loading force was adjusted between a few tens up to a few hundreds of piconewtons. The force curves were extracted from chosen area from the PFQNM images using the Peak Force Capture option from the Nanoscope software. Because of the geometry of the tip which could be considered as spherical at the apex, the force curves were then fitted using the Hertz model to get the Young's modulus values for each point of the area and the Young's Modulus values for each type of cells were represented using boxplots.

For the topographical AFM measurements (height sections and counting of lamellipodia and protrusions), a minimum of 50 images were processed for each condition while regarding

the AFM migration measurements, about 50 images per condition were captured but only approximately half of them were taken into account for our migration measurements as such measurements are highly challenging since after capturing the first image, the cell is often out of the field of view on the second image.

Videomicroscopy imaging

To measure velocity of MDA-MB-231 cells, the cells were seeded on type I collagen or fibronectin-coated, glass-bottomed chamber slide and allowed to attach to the substrate. Cells were then observed with a x20 *magnification* objective, for 24 h using a Zeiss Axio Observer Carl Zeiss MicroImaging GmbH, Deutschland). The cells were maintained at 37°C and 5% CO2 in a temperature-controlled chamber (PECON). The data were acquired using the MetaMorph software (Roper Scientific). Cell speed and directional persistence analysis were performed using ImageJ software (National Institutes of Health, Bethesda, MD, USA). For each conditions, 48 cells have been tracked.

Rho-GTPase assay

MDA-MB-231 cells (1×10^6 per well) were grown over 48h in culture plate coated with, fibronectin or type I collagen- until 90% of confluency. Then cells were lysed and Rho-GTPase activity was determined using an Active Rho Pull-Down and Detection Kit (Thermofisher, Pierce Biotechnology, USA, ref 16116) following the provider instructions.

Statistics

All the results are means ± SEM raised from two or three independent experiments. Statistical significance of differences was calculated using Two sample *t*-test or Mann Withney-U test assays (Prism software; GraphPad). *P* values referring to corresponding controls are indicated in Figure legends. *$P < 0.05$; **$P < 0.01$; ***$P < 0.001$; NS = non-significant.

Results

In order to evaluate the effect of the LRP-1 on breast cancer cells behavior, type I collagen and fibronectin coatings were used. These two ECM glycoproteins are present in breast cancer tumor microenvironment and regulate expression and activation of specific cell receptors and downstream signaling.

LRP-1 silencing in breast cancer cells

In order to study the effect of LRP-1 in breast cancer cells, MDA-MB-231 cells were -transfected to stably express a shRNA directed against LRP-1 mRNA (shLRP-1) or an shRNA with no target (shCTRL). As shown in figure 1, RT-qPCR (Fig1A) and western blot (Fig 1B) experiments revealed a decrease of the expression of LRP-1 by 60% (mRNA) and by 67% (protein). Thus, this model was used for the different experiments.

Young's moduli calculation

Our measurements were performed on type I collagen and fibronectin. As shown on Figure 2A, the Young's modulus was found to be remarkably stable on control cells with values of 2.05 +/- 0.8 kPa, and 2.06 +/- 1.03 kPa on collagen and fibronectin, respectively. In LRP-1 silenced cells, the Young's modulus dramatically increased: 5.95 +/- 2.08, and 5.03 +/- 1.84 kPa on type I collagen and fibronectin, respectively (Figure 2A). Figure 2B shows Young´s modulus mapping on shCtrl MDA-MB-231 cells (Fig 2B panel 1) and on LRP-1 silenced MDA-MB-231 cells (Fig 2B panel 2). The darker part of image which corresponds to the softer material, is mainly localized in the center of the cell. Lamellipodia and filopodia of shCtrl cells exhibit a higher stiffness compared to the cell body. LRP-1-deficient cells exhibit a stretch phenotype associated with stiff cytoplasmic extensions.

Topographical measurements

LRP-1 silencing consequences in MDA-MB-231 cells were further evaluated by topographical measurements (surface and height section). As shown in Figure 3, in the case of type I collagen, LRP-1 invalidation led to a flattening effect of the cells (8.7 +/- 2.3 µm for shCtrl cells and 6.6 +/- 1.9 µm for shLRP-1 cells). This came with an increase of the average surface (584.6 +/- 62.1 μm^2 for control cells and 778.4 +/- 83.1 μm^2 for shLRP-1 cells). Interestingly, this effect was not significant on fibronectin-coated plates.

Cell speed and directional measurements

As the correlation between the Young's modulus and cell migration is well documented [43, 44], time-lapse microscopy experiments were performed during 24 hrs to estimate velocity and direction of shCtrl and shLRP-1 cells seeded onto either type I collagen or fibronectin. As shown in Figure 4A, shCtrl cells seeded onto collagen exhibit a high directional persistence, the highest velocity (0.729 µm/min) and the highest traveled distance (1051 µm/24 hrs). Indeed, onto fibronectin, shCtrl cells exhibits a lower speed (0.414 µm/min), a lower traveled distance (596 µm/24 hrs) as well as a lower directional persistence compared to shLRP-1 cells. LRP-1 silencing impaired cell migration on both substrates with a more pronounced effect on collagen (speed: 0.412 µm/min, traveled distance: 593 µm/24 hrs) compared to fibronectin (speed: 0.290 µm/min, traveled distance 418 µm/24 hrs) (Figure 4B). It can be noticed that approximately 20% of shLRP-1 cells seeded onto fibronectin, kept a behavior close to shCtrl cells.

Migration speed measurements and topographical information obtained by AFM

Traditionally, cell migration speed is measured by video-microscopy experiments as proceeded above. Nevertheless, in these experiments, only the cell core is taken as a reference spot and over a large period of time (usually 24 hours). To provide complementary information to video-microscopy, AFM was performed as it allows to follow the cell

dynamics with high resolution. AFM experiments were then carried out by focusing on membrane extension dynamics at migration front and retraction tails (which is not possible in video-microscopy, since the cells move too fast). Figure 5A panels 1&2 and Figure 5B focused on the retraction tail dynamics. On control conditions, cell tails were found to retract quite quickly on type I collagen (1.18 +/- 0.29 µm/min) and slightly slower on fibronectin (0.83 +/- 0.12 µm/min). LRP-1 silencing led to a spectacular drop in the migration speed, on collagen (0.35 +/- 0.34 µm/min), and to a minor extent on fibronectin (0.39 +/- 0.25 µm/min). The measurements taken on the migration fronts (Figure 5A panels 3&4, Figure 5B) led to similar observations: control cells were able to move quite fast on the two substrates (1.08 +/- 0.15 µm/min on collagen, and 0.79 +/- 0.18 µm/min on fibronectin). This time, LRP-1 invalidation led to a spectacular decrease in the migration capabilities on the fibronectin (0.24 +/- 0.01 µm/min) and with a less extent on collagen (0.51 +/- 0.09 µm/min). The clear morphological differences obtained between shCtrl and shLRP-1 cells on collagen prompted us to investigate more in details the height images obtained on this substrate, particularly the number of filopodiae and protrusions at the migration front. Figure 6-panel 1 shows a typical migration front where the filopodia can be numbered, and Figure 6-panel 2, a typical cross-section achieved on a protrusion. The number of filopodiae on type I collagen (Table 1) was quite similar between the control (12) and the LRP-1-silenced (13.5) cells as well as the number of membrane protrusions (27.7 for the shCtrl cells and 21.1 for the shLRP-1 cells). On the other hand, the average height of the protrusions was systematically found to be more important on shCtrl (381.9 nm on collagen) than on shLRP-1 (269 nm on collagen) cells. Taken together, those results tend to prove that the membrane remodeling at the leading edge of shCtrl and shLRP-1 cells seeded onto type I collagen is quite similar. Considering the obtained data, additional experiments were carried out by assaying Rho-

GTPase protein activities, molecular actors involved in the regulation of actin cytoskeleton dynamics.

Rho-GTPases assay

Rho GTPases include Rho, Rac and CDC42 proteins known to be mainly involved in cell migration and morphology especially by controlling the dynamic of actin cytoskeleton. Rho GTPase activity is regulated by GDP (inactive state) and GTP (active state). Activated Rho GTPases are able to interact with specific signaling molecules and induce downstream signaling [45].

In order to establish a potential correlation between AFM and time-lapse microscopy analyses, immunoprecipitation of Rho GTPases in shCtrl and shLRP-1 cells was also performed. As shown in Figure 7, we observed a decrease of 50% of the Rho GTPase activity when LRP-1 was silenced, only when cells were seeded onto fibronectin. These results corroborate the decrease of cell migration observed in time-lapse microscopy (Figure 4) as well as the decrease of membrane dynamics observed using AFM at the leading edge of the cells (Figure 5).

Immunofluorescence experiments

To go deeper in the understanding of these observations, immunofluorescence experiments were also performed and actin microfilaments and talin were labelled to visualize actin cytoskeleton extensions and focal adhesion contacts, respectively.

As shown in Figure 8, the morphology of shCtrl cells was quite similar on both type-I collagen and fibronectin with a developed actin cytoskeleton associated to focal contacts at the leading edge (Figs. 8A, 8B). Nevertheless, cells seeded onto collagen exhibited a polarized phenotype associated with numerous focal adhesion contacts at the leading edge (Fig 8A, panels 1&3) as shown by co-localized voxels between actin and talin (Fig 8A, panels 5,

arrows). Concerning the shLRP-1 cells, striking differences were observed on collagen associated with a thin stretch phenotype ((Fig. 8A, panels 2,4) containing focal contact at each side of the cell (Fig. 8A, panel 6, arrows). LRP-1 silencing also affects cell morphology when cells are seeded on fibronectin (Fig 8B). Indeed, LRP-1-silenced cells adopted a more stretched phenotype (Fig. 8B, panels 2, 4), however the cell polarity seemed to be preserved. The intensity and size of focal contact decrease as observed in Fig 8B (panel 6 vs panel 5, arrows).

Discussion

Triple negative breast cancer (TNBC) counts among the more aggressive breast cancer [46].It constitutes an essential challenge to identify molecular regulators involved in cancer cell migration and/or invasion as these processes represent key steps in the process of tumor cell dissemination to establish metastasis [47]. Among these molecular actors, LRP-1, an endocytic scavenger receptor already described for its role in cancer progression [48], seems to support pro-tumor functionalities in breast cancers [48].

The aim of our study was to evaluate the role of LRP-1 on elasticity, migration and spreading of MDA-MB-231 breast cancer cells seeded on both type-I collagen and fibronectin. These two glycoproteins represent the major components of breast cancer tumor microenvironment [49]. Indeed, type I collagen constitutes the scaffold of tumor microenvironment and can promote tumor infiltration, angiogenesis, invasion and migration [50]. Fibronectin in turn is a primary component of the mammary mesenchymal compartment [51]. Its expression represents a robust indicator of lymph node involvement and is also correlated to mortality risk [52]. In this context, AFM approaches in PeakForce QNM mode were used to study live cells [41]. The Young's modulus from shCtrl cells reaches 2.0 kPa on both fibronectin and type I collagen. Interestingly, Teng et al. have previously

reported a Young's modulus of 1.1 kPa and 2.2 kPa for MDA-MB-231 seeded on collagen and fibronectin, respectively [53]. These authors have performed a recording in the vicinity of the nucleus and have shown that fibronectin induced an increase of the mean young modulus compared to type I collagen. In our study, QNM acquisitions were achieved everywhere on the cell with due respect of a recorded zone at least 4 times superior to the indentation depth. Regarding the results obtained in LRP-1-silenced cells, a significant increase of the Young's modulus was measured, that reached 5.95 and 5.03 kPa onto collagen and fibronectin, respectively. Numerous studies have reported that the increase of cellular stiffness is related to a less invasive phenotype [54].

These data suggest, in accordance with our previous studies performed on FTC-133 thyroid carcinoma cells [14, 38], that LRP-1 silencing appears correlated to an impaired ability for the cells to deform and migrate. When type I collagen was used as a coating, LRP-1 invalidation led to a flattening effect and an increase of the average cell surface. Interestingly, no significant difference was observed on fibronectin-coated plates, in terms of height section and surface. These observations could be linked to the high spread of shCtrl cells on fibronectin. Our results indicated that LRP-1-expressing breast tumor cells seeded onto collagen exhibited a higher directional persistence as well as a higher velocity compared to cells seeded onto fibronectin. Considering these results, collagen which is found in breast cancer tumor microenvironment, represents a privileged guide for cell dissemination, that participates in the increase of cell aggressiveness [55]. LRP-1 silencing reduced cell velocity by 45% (24.7 μm/h) and 30% (17.4 μm/h) on collagen and fibronectin respectively which is in line with the Young modulus variations determined by AFM (Fig. 2). Nevertheless, an important observation in our study concerns the fact that the Young modulus value of MDA-MB-231 is quite identical on type I collagen and fibronectin whereas tumor cells have a

different behavior on these two matrix associated substrates. Lekka have already pointed out the fact that Young modulus is not sufficient by itself to explain/characterize cell behavior [54]. To complement our measurements, AFM was used to focus on different cell parts, like the migration front or the retraction. It was demonstrated that the tails of the control cells retract quite quickly on type I collagen (1.18 µm/min) and slightly slower on fibronectin (0.83 µm/min). As for the LRP-1 silencing cells, we measured a spectacular drop in the migration speed at the tail extension, by 2.7 fold on collagen (0.35 µm/min), and a minor extent on fibronectin (by 2.1 fold to 0.39 µm/min). At the migration front, LRP-1 invalidation led to a substantial decrease of the migration abilities of the cells on fibronectin (by 3.6 fold to 0.24 µm/min) and to a slightly lesser extent on collagen (by 2.1 fold to 0.51 µm/min). Actin microfilament and talin labelling, pointed out the fact that the morphologies of breast cancer cells are quite similar on both collagen and fibronectin with a well-developed actin cytoskeleton associated with focal contacts at the leading edge. However, the morphology of tumor cells on type I collagen seems to be more polarized and that could explain the highest migration speed on this substrate. When LRP-1 is silenced, striking differences are observed for cell morphology onto collagen with a stretch phenotype and a loss of the polarized extensions. These effects are less pronounced in shLRP-1 cells seeded on fibronectin than shCtrl cells and corroborate with the cell velocity data (Fig. 7 and Fig.8). To investigate more precisely the dynamic of cytoskeleton, Rho GTPase activities were investigated. This family is represented by Rho, Rac and CDC42 proteins, and is involved in cell migration and morphology by controlling the dynamic of actin cytoskeleton [56]. Previous results obtained on Schwann cells have demonstrated the ability of LRP-1 to regulate these proteins [57] Interestingly, a decrease by 50% of Rho GTPase activity was observed in LRP-1-deficient cells cultured onto fibronectin which can be correlated to the

results obtained using AFM and videomicroscopy (Fig.2 and Fig. 4). When cells are cultured on type I collagen, no significant modification were observed when LRP-1 was silenced. It is worth to mention that our study measured the global activity of RhoGTPases and not only Rho. It could be of interest to focus only on Rho proteins and their associated kinases. Moreover, RhoA was usually maximally activated to nearby to the leading edge [58].

By looking at the results of immunofluorescence more closely, it seems that shLRP-1 cells seeded on collagen lost their polarity and turned out to be characterized by two leading edges inducing a migration way in opposite direction without efficient movement. These observations have been corroborated by time lapse study (see supplementary video files).

In conclusion, our study demonstrates thanks to a multi-technique approach focusing on AFM measurements that LRP-1 acts as a pro-migratory actor in MDA-MB-231 cells and that extracellular proteins found in breast microenvironment such as fibronectin or type I collagen are able to modulate this effect.

Acknowledgments

The authors thank the Region Champagne Ardenne, URCA, DRRT Grand Est and FEDER program. The video microscopy and confocal microscopy experiments were performed at the PICT platform, URCA, with assistance from Christine Terryn and Arnaud Bonnomet. The AFM experiments were performed in the NanoMat' facility. The authors would like to thank Cathy Hachet for her technical assistance. Graphical abstract was realized with the help of Adrien Dos Santos.

References

1 A. P. Lillis, M. C. Greenlee, I. Mikhailenko, S. V. Pizzo, A. J. Tenner, D. K. Strickland, and S. S. Bohlson, Murine low-density lipoprotein receptor-related protein 1 (LRP) is required for phagocytosis of targets bearing LRP ligands but is not required for C1q-triggered enhancement of phagocytosis. *J Immunol*. 181, 364-73 **(2008)**

2 S. L. Gonias, and W. M. Campana, LDL receptor–related protein-1: a regulator of inflammation in atherosclerosis, cancer, and injury to the nervous system. *The American journal of pathology*. 184, 18-27 **(2014)**

3 D. K. Strickland, D. T. Au, P. Cunfer, and S. C. Muratoglu, Low-density lipoprotein receptor-related protein-1: role in the regulation of vascular integrity. *Arterioscler Thromb Vasc Biol*. 34, 487-98 **(2014)**

4 Y. Zhao, D. Li, J. Zhao, J. Song, and Y. Zhao, The role of the low-density lipoprotein receptor-related protein 1 (LRP-1) in regulating blood-brain barrier integrity. *Rev Neurosci*. 27, 623-34 **(2016)**

5 L. M. Landowski, M. Pavez, L. S. Brown, R. Gasperini, B. V. Taylor, A. K. West, and L. Foa, Low-density Lipoprotein Receptor-related Proteins in a Novel Mechanism of Axon Guidance and Peripheral Nerve Regeneration. *J Biol Chem*. 291, 1092-102 **(2016)**

6 V. Llorente-Cortes, V. Barbarigo, and L. Badimon, Low density lipoprotein receptor-related protein 1 modulates the proliferation and migration of human hepatic stellate cells. *J Cell Physiol*. 227, 3528-33 **(2012)**

7 R. K. Kancha, M. E. Stearns, and M. M. Hussain, Decreased expression of the low density lipoprotein receptor-related protein/alpha 2-macroglobulin receptor in invasive cell clones derived from human prostate and breast tumor cells. *Oncol Res*. 6, 365-72 **(1994)**

8 R. R. Desrosiers, M. E. Rivard, P. E. Grundy, and B. Annabi, Decrease in LDL receptor-related protein expression and function correlates with advanced stages of Wilms tumors. *Pediatr Blood Cancer*. 46, 40-9 **(2006)**

9 K. Obermeyer, S. Krueger, B. Peters, B. Falkenberg, A. Roessner, and C. Rocken, The expression of low density lipoprotein receptor-related protein in colorectal carcinoma. *Oncol Rep*. 17, 361-7 **(2007)**

10 C. Boulagnon-Rombi, C. Schneider, C. Leandri, A. Jeanne, V. Grybek, A. M. Bressenot, C. Barbe, B. Marquet, S. Nasri, and C. Coquelet, LRP1 expression in colon cancer predicts clinical outcome. *Oncotarget*. 9, 8849 **(2018)**

11 C. Foca, E. K. Moses, M. A. Quinn, and G. E. Rice, Differential expression of the alpha(2)-macroglobulin receptor and the receptor associated protein in normal human endometrium and endometrial carcinoma. *Mol Hum Reprod*. 6, 921-7 **(2000)**

12 X. Song, J. B. Wang, D. L. Yin, H. Y. Yang, L. X. Liu, and H. C. Jiang, Down-regulation of lung resistance related protein by RNA interference targeting survivin induces the reversal of chemoresistances in hepatocellular carcinoma. *Chin Med J (Engl)*. 122, 2636-42 **(2009)**
13 B. Sid, S. Dedieu, N. Delorme, H. Sartelet, G. M. Rath, G. Bellon, and L. Martiny, Human thyroid carcinoma cell invasion is controlled by the low density lipoprotein receptor-related protein-mediated clearance of urokinase plasminogen activator. *Int J Biochem Cell Biol*. 38, 1729-40 **(2006)**
14 S. Dedieu, B. Langlois, J. Devy, B. Sid, P. Henriet, H. Sartelet, G. Bellon, H. Emonard, and L. Martiny, LRP-1 silencing prevents malignant cell invasion despite increased pericellular proteolytic activities. *Mol Cell Biol*. 28, 2980-95 **(2008)**
15 Y. Li, N. Wood, P. Grimsley, D. Yellowlees, and P. K. Donnelly, In vitro invasiveness of human breast cancer cells is promoted by low density lipoprotein receptor-related protein. *Invasion Metastasis*. 18, 240-51 **(1998)**
16 B. Fayard, F. Bianchi, J. Dey, E. Moreno, S. Djaffer, N. E. Hynes, and D. Monard, The serine protease inhibitor protease nexin-1 controls mammary cancer metastasis through LRP-1–mediated MMP-9 expression. *Cancer research*. 69, 5690-5698 **(2009)**
17 L. Theret, A. Jeanne, B. Langlois, C. Hachet, M. David, M. Khrestchatisky, J. Devy, E. Hervé, S. Almagro, and S. Dedieu, Identification of LRP-1 as an endocytosis and recycling receptor for β1-integrin in thyroid cancer cells. *Oncotarget*. 8, 78614 **(2017)**
18 D. Berk, and E. Evans, Detachment of agglutinin-bonded red blood cells. III. Mechanical analysis for large contact areas. *Biophys J*. 59, 861-72 **(1991)**
19 K. Tsukada, E. Sekizuka, C. Oshio, and H. Minamitani, Direct measurement of erythrocyte deformability in diabetes mellitus with a transparent microchannel capillary model and high-speed video camera system. *Microvasc Res*. 61, 231-9 **(2001)**
20 *Feeling for cells with light*. Proceedings of the Optical Trapping and Optical Micromanipulation, **(2004)**;
21 A. R. Bausch, F. Ziemann, A. A. Boulbitch, K. Jacobson, and E. Sackmann, Local measurements of viscoelastic parameters of adherent cell surfaces by magnetic bead microrheometry. *Biophys J*. 75, 2038-49 **(1998)**
22 N. Wang, E. Ostuni, G. M. Whitesides, and D. E. Ingber, Micropatterning tractional forces in living cells. *Cell Motil Cytoskeleton*. 52, 97-106 **(2002)**
23 E. P. Wojcikiewicz, X. Zhang, and V. T. Moy, Force and Compliance Measurements on Living Cells Using Atomic Force Microscopy (AFM). *Biol Proced Online*. 6, 1-9 **(2004)**
24 M. Radmacher, Studying the mechanics of cellular processes by atomic force microscopy. *Methods Cell Biol*. 83, 347-72 **(2007)**
25 M. E. Dokukin, N. V. Guz, and I. Sokolov, Quantitative study of the elastic modulus of loosely attached cells in AFM indentation experiments. *Biophys J*. 104, 2123-31 **(2013)**
26 N. Guz, M. Dokukin, V. Kalaparthi, and I. Sokolov, If cell mechanics can be described by elastic modulus: study of different models and probes used in indentation experiments. *Biophysical journal*. 107, 564-575 **(2014)**
27 G. Binnig, C. F. Quate, and C. Gerber, Atomic force microscope. *Phys Rev Lett*. 56, 930-933 **(1986)**
28 I. Sokolov, S. Iyer, and C. D. Woodworth, Recovery of elasticity of aged human epithelial cells in vitro. *Nanomedicine*. 2, 31-6 **(2006)**
29 C. Callies, J. Fels, I. Liashkovich, K. Kliche, P. Jeggle, K. Kusche-Vihrog, and H. Oberleithner, Membrane potential depolarization decreases the stiffness of vascular endothelial cells. *J Cell Sci*. 124, 1936-42 **(2011)**
30 M. Lekka, P. Laidler, D. Gil, J. Lekki, Z. Stachura, and A. Z. Hrynkiewicz, Elasticity of normal and cancerous human bladder cells studied by scanning force microscopy. *Eur Biophys J*. 28, 312-6 **(1999)**
31 M. J. Rosenbluth, W. A. Lam, and D. A. Fletcher, Force microscopy of nonadherent cells: a comparison of leukemia cell deformability. *Biophys J*. 90, 2994-3003 **(2006)**
32 S. E. Cross, Y. S. Jin, J. Rao, and J. K. Gimzewski, Nanomechanical analysis of cells from cancer patients. *Nat Nanotechnol*. 2, 780-3 **(2007)**

33 E. Henderson, P. G. Haydon, and D. S. Sakaguchi, Actin filament dynamics in living glial cells imaged by atomic force microscopy. *Science*. 257, 1944-6 **(1992)**
34 Q. Zhong, D. Inniss, K. Kjoller, and V. Elings, Fractured polymer/silica fiber surface studied by tapping mode atomic force microscopy. *Surface Science Letters*. 290, L688-L692 **(1993)**
35 J. H. Hoh, and C. A. Schoenenberger, Surface morphology and mechanical properties of MDCK monolayers by atomic force microscopy. *J Cell Sci*. 107 (Pt 5), 1105-14 **(1994)**
36 C. Rotsch, and M. Radmacher, Drug-induced changes of cytoskeletal structure and mechanics in fibroblasts: an atomic force microscopy study. *Biophys J*. 78, 520-35 **(2000)**
37 *Expression of Tumor Suppressors PTEN and TP53 in Isogenic Glioblastoma U-251MG Cells Affects Cellular Mechanical Properties—An AFM-Based Quantitative Investigation*. Proceedings of the JJAP Conference Proceedings, **(2013)**;
38 A. Le Cigne, L. Chieze, A. Beaussart, S. El-Kirat-Chatel, Y. F. Dufrene, S. Dedieu, C. Schneider, L. Martiny, J. Devy, and M. Molinari, Analysis of the effect of LRP-1 silencing on the invasive potential of cancer cells by nanomechanical probing and adhesion force measurements using atomic force microscopy. *Nanoscale*. 8, 7144-54 **(2016)**
39 D. Alsteens, V. Dupres, S. Yunus, J.-P. Latgé, J. r. J. Heinisch, and Y. F. Dufrêne, High-resolution imaging of chemical and biological sites on living cells using peak force tapping atomic force microscopy. *Langmuir*. 28, 16738-16744 **(2012)**
40 B. Pittenger, N. Erina, and C. Su, Quantitative mechanical property mapping at the nanoscale with PeakForce QNM. *Application Note Veeco Instruments Inc*. 1-2 **(2010)**
41 C. Heu, A. Berquand, C. Elie-Caille, and L. Nicod, Glyphosate-induced stiffening of HaCaT keratinocytes, a Peak Force Tapping study on living cells. *J Struct Biol*. 178, 1-7 **(2012)**
42 I. N. Sneddon, The relation between load and penetration in the axisymmetric Boussinesq problem for a punch of arbitrary profile. *International journal of engineering science*. 3, 47-57 **(1965)**
43 M. Nagayama, H. Haga, and K. Kawabata, Drastic change of local stiffness distribution correlating to cell migration in living fibroblasts. *Cytoskeleton*. 50, 173-179 **(2001)**
44 T. G. Kuznetsova, M. N. Starodubtseva, N. I. Yegorenkov, S. A. Chizhik, and R. I. Zhdanov, Atomic force microscopy probing of cell elasticity. *Micron*. 38, 824-833 **(2007)**
45 A. J. Ridley, Rho GTPase signalling in cell migration. *Current opinion in cell biology*. 36, 103-112 **(2015)**
46 P. Khosravi-Shahi, L. Cabezon-Gutierrez, and S. Custodio-Cabello, Metastatic triple negative breast cancer: Optimizing treatment options, new and emerging targeted therapies. *Asia Pac J Clin Oncol*. 14, 32-39 **(2018)**
47 A. J. Redig, and S. S. McAllister, Breast cancer as a systemic disease: a view of metastasis. *J Intern Med*. 274, 113-26 **(2013)**
48 V. Montel, A. Gaultier, R. D. Lester, W. M. Campana, and S. L. Gonias, The low-density lipoprotein receptor-related protein regulates cancer cell survival and metastasis development. *Cancer Res*. 67, 9817-24 **(2007)**
49 C. Robertson, The extracellular matrix in breast cancer predicts prognosis through composition, splicing, and crosslinking. *Exp Cell Res*. 343, 73-81 **(2016)**
50 M. Fang, J. Yuan, C. Peng, and Y. Li, Collagen as a double-edged sword in tumor progression. *Tumour Biol*. 35, 2871-82 **(2014)**
51 C. L. Li, D. Yang, X. Cao, F. Wang, D. Y. Hong, J. Wang, X. C. Shen, and Y. Chen, Fibronectin induces epithelial-mesenchymal transition in human breast cancer MCF-7 cells via activation of calpain. *Oncol Lett*. 13, 3889-3895 **(2017)**
52 M. M. Mohamed, D. Al-Raawi, S. F. Sabet, and M. El-Shinawi, Inflammatory breast cancer: New factors contribute to disease etiology: A review. *J Adv Res*. 5, 525-36 **(2014)**
53 Y. Teng, J. Qiu, Y. Zheng, X. Luo, L. Zhang, L. Chen, and G. Wang, Effects of type I collagen and fibronectin on regulation of breast cancer cell biological and biomechanical characteristics. *J Med Biol Eng*. 34, 62-68 **(2014)**
54 M. Lekka, Discrimination Between Normal and Cancerous Cells Using AFM. *Bionanoscience*. 6, 65-80 **(2016)**

55 T. Yu, and G. Di, Role of tumor microenvironment in triple-negative breast cancer and its prognostic significance. *Chin J Cancer Res*. 29, 237-252 **(2017)**
56 N. Tapon, and A. Hall, Rho, Rac and Cdc42 GTPases regulate the organization of the actin cytoskeleton. *Curr Opin Cell Biol*. 9, 86-92 **(1997)**
57 E. Mantuano, M. Jo, S. L. Gonias, and W. M. Campana, Low density lipoprotein receptor-related protein (LRP1) regulates Rac1 and RhoA reciprocally to control Schwann cell adhesion and migration. *Journal of Biological Chemistry*. 285, 14259-14266 **(2010)**
58 M. Machacek, L. Hodgson, C. Welch, H. Elliott, O. Pertz, P. Nalbant, A. Abell, G. L. Johnson, K. M. Hahn, and G. Danuser, Coordination of Rho GTPase activities during cell protrusion. *Nature*. 461, 99-103 **(2009)**

Figures legends

Figure 1: Short hairpin LRP-1 strategy induced LRP-1 silencing in triple negative breast cancer cell line (MDA-MB-231) (A) transcriptional level of LRP-1 was assessed by RTqPCR. Level of LRP-1 mRNA expression in shCtrl was fixed arbitrary at 100%. (B) whole cell extracts from shCtrl and shLRP-1 were analysed by SDS PAGE followed by western blotting using an anti-LRP-1 and anti-GAPDH antibodies (Left panel). Graphical representation of LRP-1 protein expression normalized with GAPDH (Right panel). Data are representative of three separate experiments. **p <0.01 (t-test).

Figure 2. **LRP-1 silencing in MDA-MB-231 leads to an increase of the Young's modulus by 2.5 to 3-fold on type I collagen and fibronectin.**

(A) Quantification of the average Young's modulus of shCtrl and shLRP-1 cells seeded onto collagen and fibronectin. (B) Mapping of the Young's modulus obtained by PFQNM for shCtrl (1) and shLRP-1 (2) MDA-MBA-231 cells seeded on type I collagen. To emphasize the differences, a logarithm scale is used. Corresponding peak force error images, related to the topography changes, are shown in inset. *** p<0.001 (Mann Whitney-U test)

Figure 3: Topographical AFM measurements of MDA-MB-231 cells on type I collagen, and fibronectin. The height section, measured on collagen (black) and fibronectin (crosslines), is significantly decreased on collagen when LRP-1 was silenced. This is correlated with an increased spreading capacity of the cells. * $p<0.05$, ** $p<0.01$, NS Non Significant (t-test).

Figure 4 LRP-1 silencing in MDA-MB-231 decreases the cell speed and impairs directional persistence. (A) Full trajectory of shCTRL cell (left column) and shLRP cells (right column) seeded on type I collagen (upper lane) and fibronectin (bottom lane). The shCTRL cells show higher migration than the shLRP-1 over a representative nine-hour period. (B) Representative average cell speed on type collagen and fibronectin after 24 h. ** $p \leq 0.01$ (t-test).

Figure 5. LRP-1 silencing MDA-MB-231 impairs the migration speed, measured over the retraction tail and the migration front. **(A)** Peak force error images (z-scale: 0 to 50 pN) were captured on collagen coated-substrates. Nominal force (down to 10 pN) was minimized to avoid overstressing the cells. In 1 and 2 are shown 50x25 µm images of a retraction tail, with a 8 min-time difference. In 3 and 4 are shown 50x30 µm images of a migration front, with a 22 min-time difference. **(B)** migration speed on type I collagen (black) and fibronectin (crossline), for the retraction tail and the migration front.

Figure 6. LRP-1 silencing decreases the number of membrane protrusions on type collagen and fibronectin. Example of Images used to count the filopodia, protrusions and estimate the height of the protrusions. The present images give representative examples of how the

filopodia can be visualized (1) and how cross-sections can be performed on the protrusions (2).

Figure 7. LRP-1 silencing impairs RhoGTPases activities on fibronectin

Quantification of the RhoGTPases activities in MDA-MB-231 shCtrl and shLRP-1 cells seeded onto collagen and fibronectin for 24hrs Datas are representative of two separate experiments. NS. Non significant, *p<0.05 (t-test)

FIG. 8. LRP-1-silencing in MDA-MB-231 exhibits striking differences in actin cytoskeleton and focal adhesion organization. shCTRL (1, 3, 5) and shLRP-1 (2, 4, 6) cells were plated onto collagen **(A)** or fibronectin **(B)** for 24hrs before to be fixed (4% paraformaldehyde). Cells were incubated with phalloidin-alexa 488^{TM} for actin filaments staining (green) and anti-talin antibody and labelled with secondary antibody linked to Alexa 568^{TM} (red). Nuclei were counterstained with DAPI (blue). Fifteen to twenty imges were captured with a 0.25µm Z step. Images 1 and 2 correspond to a z-projection, images 3 and 4 correspond to an isosurfacic representation and images 5 and 6 show co-localized voxels between actin and talin. Images are representative of three separate experiments. Scale bar: 10µm

Table 1. Quantification of the number of membrane protrusion on collagen and fibronectin

On both substrates, the data tend to prove than the membrane remodeling is more present on control than on ShLRP-1 cells, which is a marker of higher migration capabilities.

Figure 1

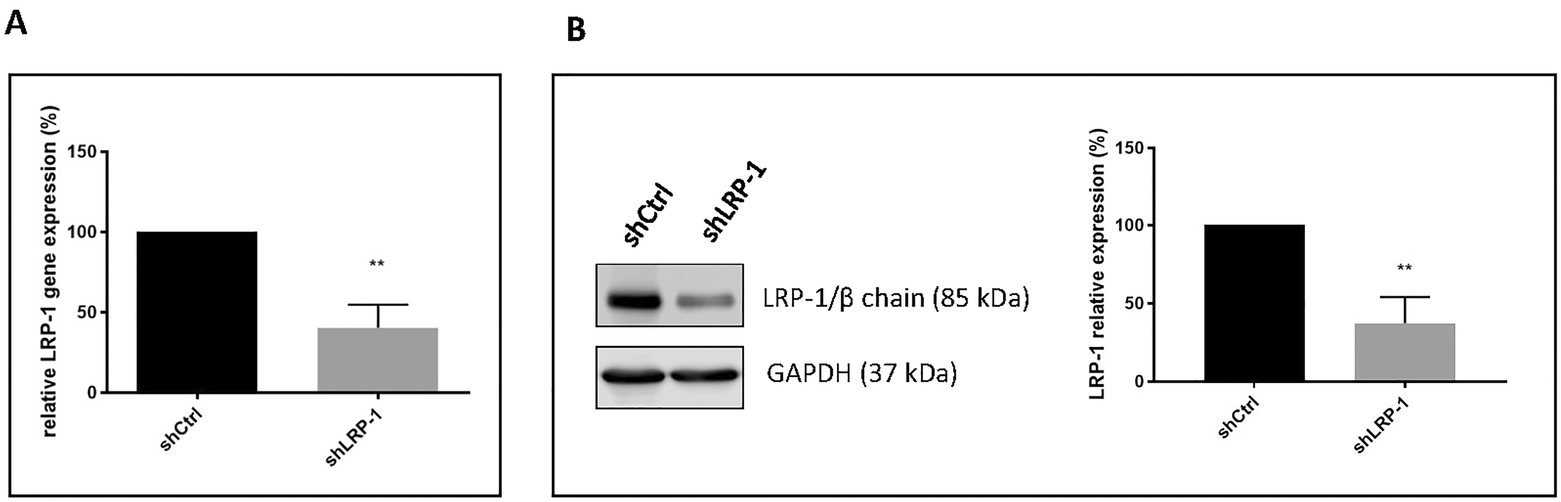
A
relative LRP-1 gene expression (%)
150
100
50
0
**
shCtrl
shLRP-1
B
shCtrl
shLRP-1
LRP-1/β chain (85 kDa)
GAPDH (37 kDa)
LRP-1 relative expression (%)
150
100
50
0
**
shCtrl
shLRP-1

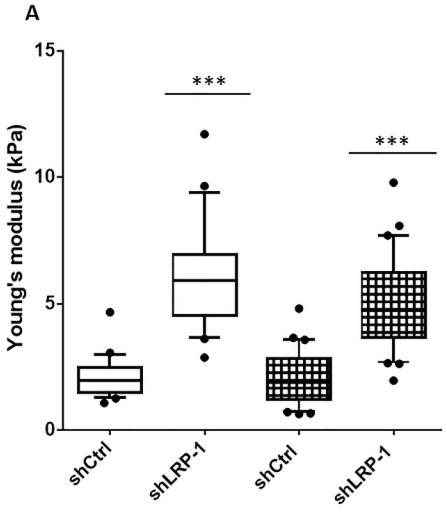
A
15
10
5
0
Young's modulus (kPa)
***
***
shCtrl
shLRP-1
shCtrl
shLRP-1

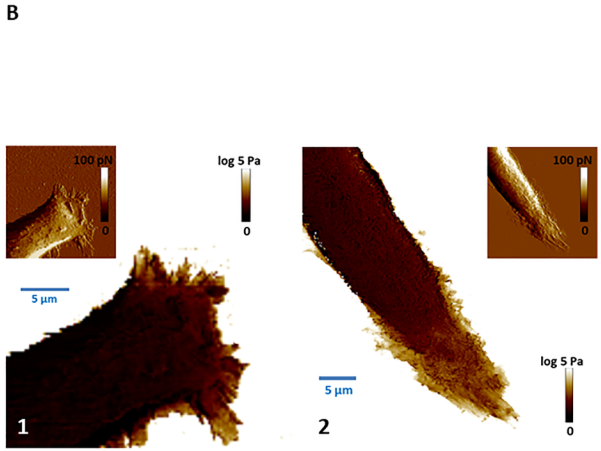
B
100 pN
0
log 5 Pa
0
5 µm
1
100 pN
0
5 µm
2
log 5 Pa
0

Figure 3

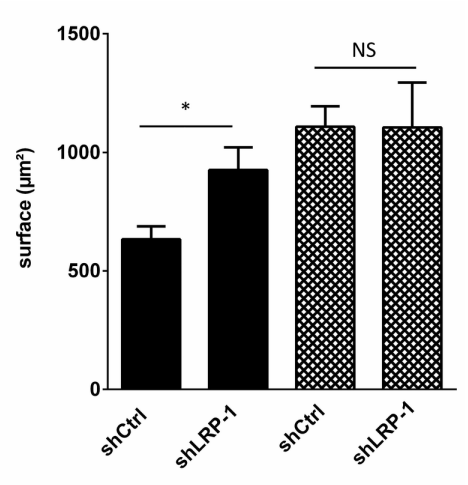
1500
1000
500
0
surface (µm²)
*
NS
shCtrl
shLRP-1
shCtrl
shLRP-1

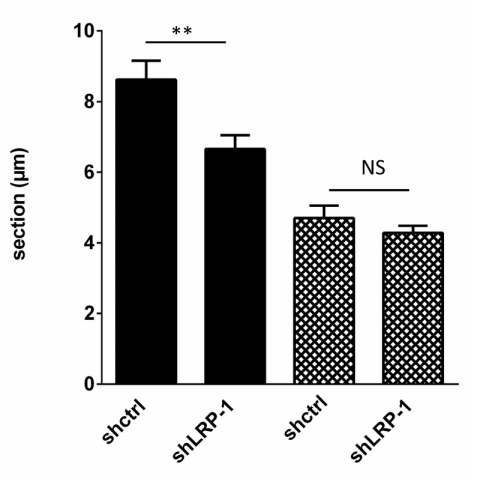
10
8
6
4
2
0
section (µm)
**
NS
shctrl
shLRP-1
shctrl
shLRP-1

Figure 4

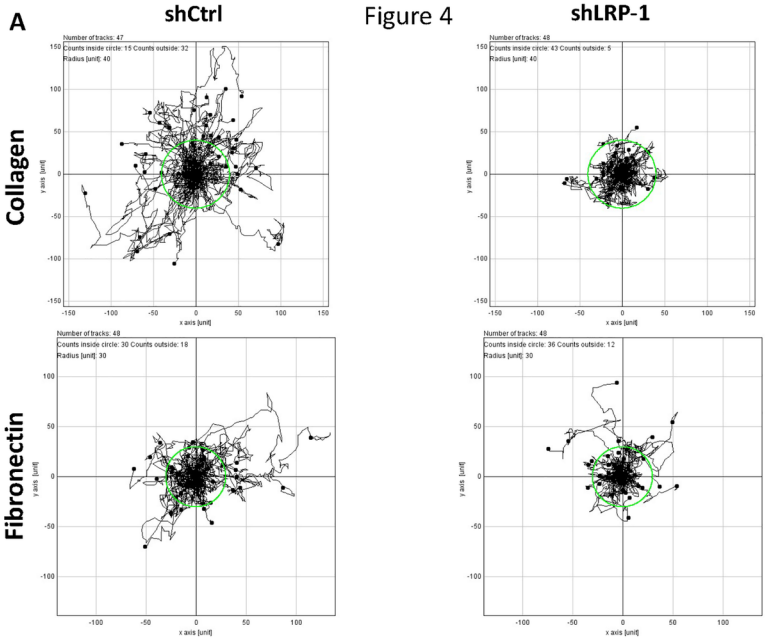
A
shCtrl
shLRP-1
Collagen
Fibronectin
Number of tracks: 47
Counts inside circle: 15 Counts outside: 32
Radius [unit]: 40
Number of tracks: 48
Counts inside circle: 43 Counts outside: 5
Radius [unit]: 40
Number of tracks: 48
Counts inside circle: 30 Counts outside: 18
Radius [unit]: 30
Number of tracks: 48
Counts inside circle: 36 Counts outside: 12
Radius [unit]: 30
x axis [unit]
y axis [unit]
B
Distance (µm)
**
**
shCtrl
shLRP-1
shCtrl
shLRP-1

A

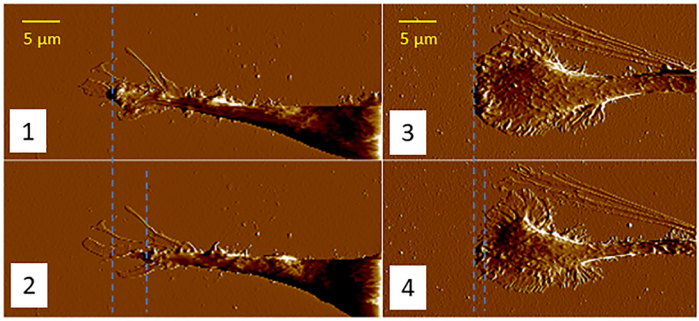
5 µm
1
2
5 µm
3
4

B

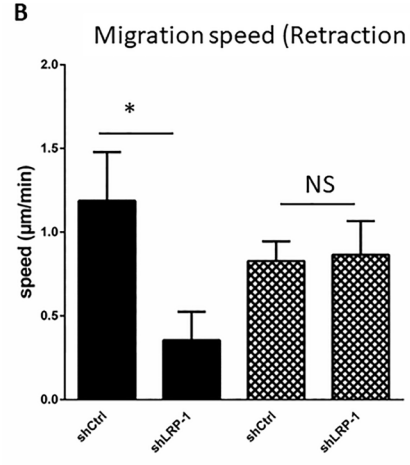
Migration speed (Retraction Tail)
speed (µm/min)
2.0
1.5
1.0
0.5
0.0
*
NS
shCtrl
shLRP-1
shCtrl
shLRP-1

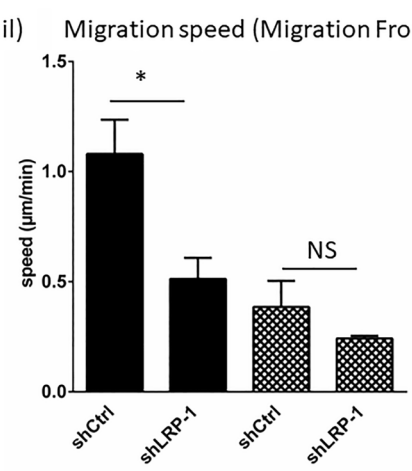
Migration speed (Migration Front)
speed (µm/min)
1.5
1.0
0.5
0.0
*
NS
shCtrl
shLRP-1
shCtrl
shLRP-1

A

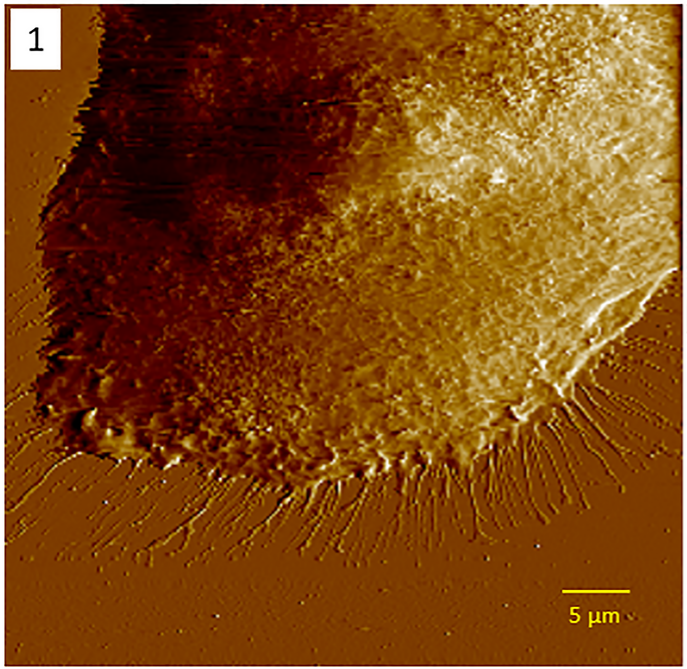

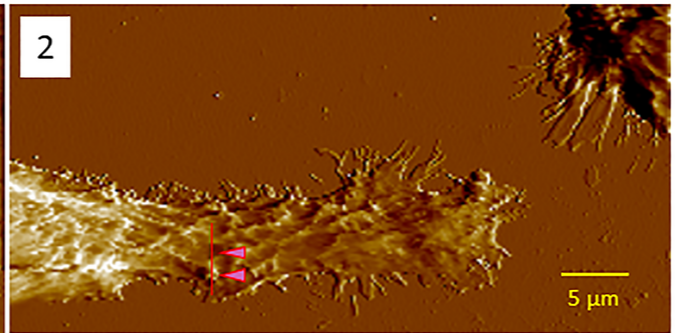

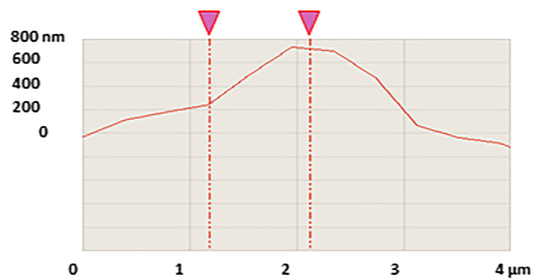

B

Sample	filopodes	protrusions	Protrusion height
Ctrl Coll	12	27,7	381,9 nm
SHLRP1 Coll	13,5	21,1	269 nm
Ctrl Fibro	33,3	22,4	319,3 nm
SHLRP1 Fibro	(ND)	14	167 nm

Figure 7

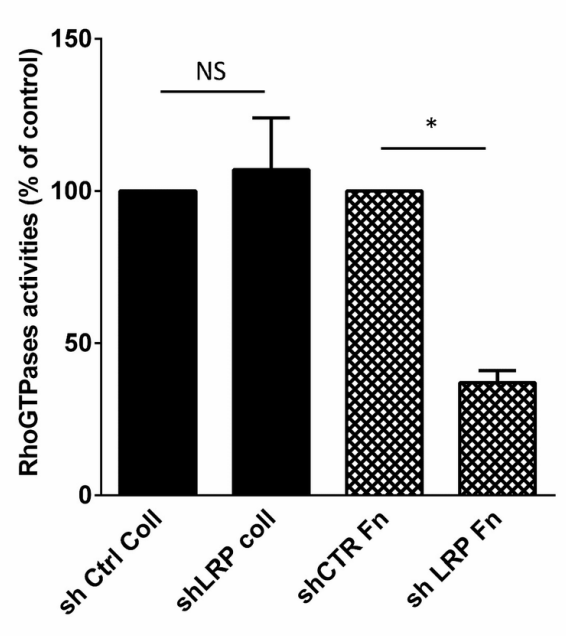
RhoGTPases activities (% of control)
150
100
50
0
NS
*
sh Ctrl Coll
shLRP coll
shCTR Fn
sh LRP Fn

Figure 8A

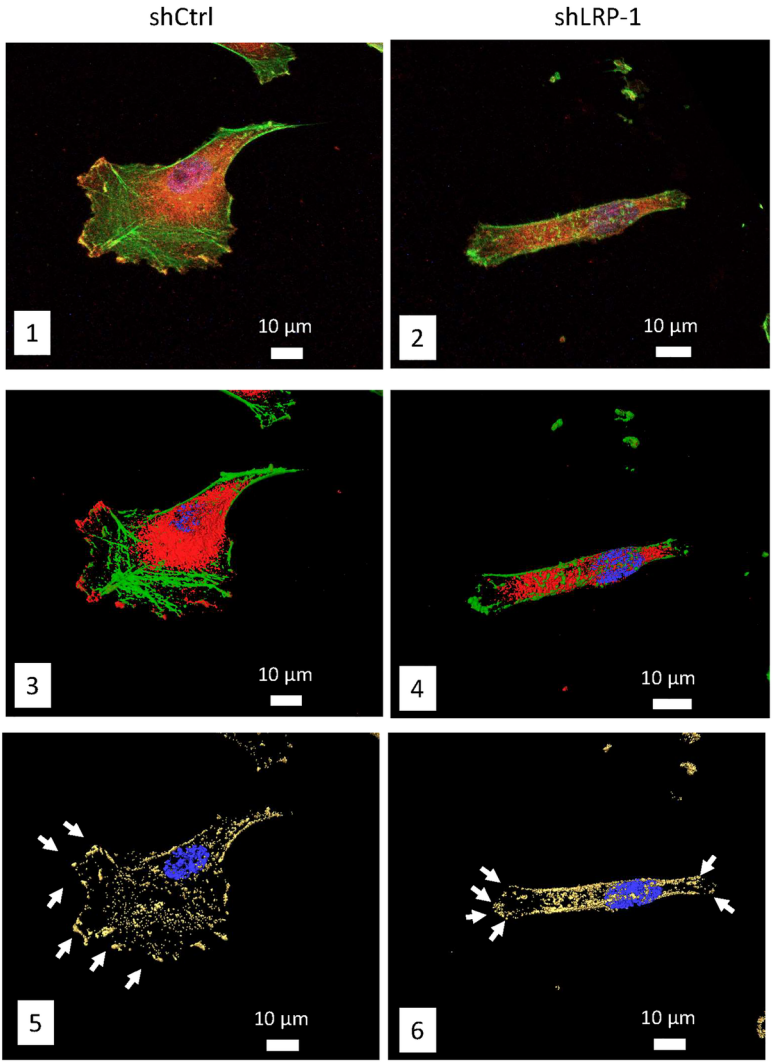
collagen
shCtrl
shLRP-1
1
10 µm
2
10 µm
3
10 µm
4
10 µm
5
10 µm
6
10 µm

Figure 8B

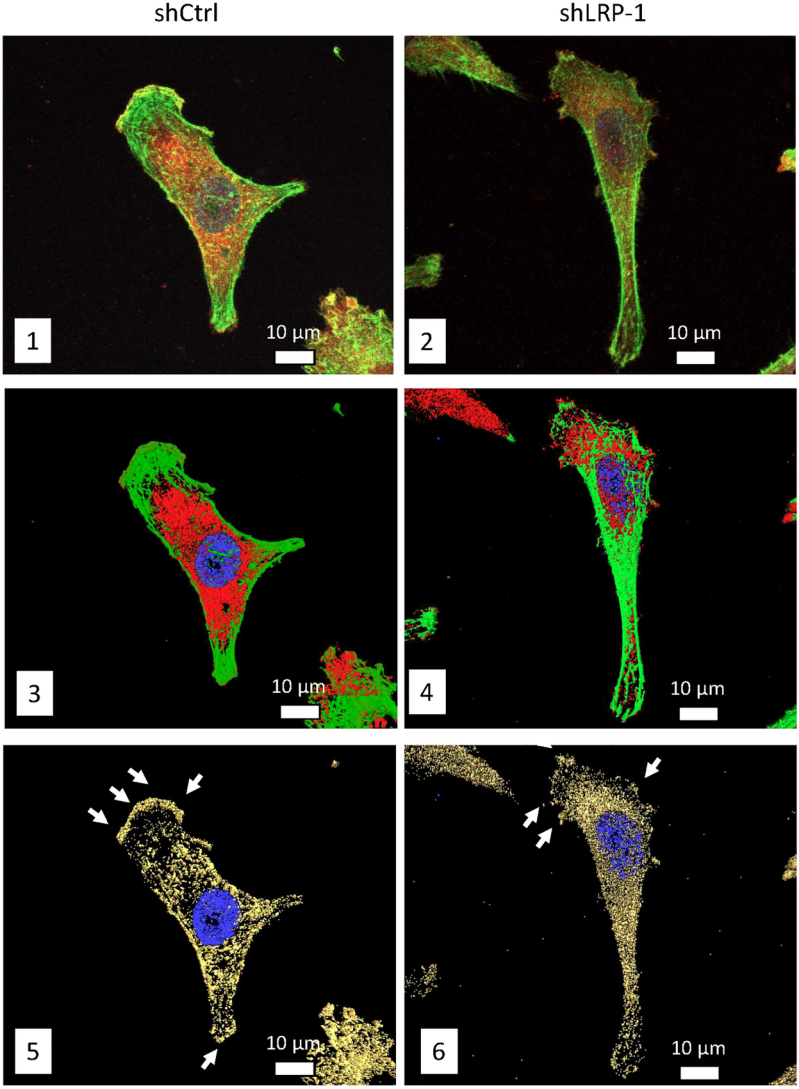
Fibronectin
shCtrl
shLRP-1
1
10 µm
2
10 µm
3
10 µm
4
10 µm
5
10 µm
6
10 µm

Table 1

Sample	filopodes	protrusions	Protrusion height
Ctrl Coll	12	27,7	381,9 nm
SHLRP1 Coll	13,5	21,1	269 nm
Ctrl Fibro	33,3	22,4	319,3
SHLRP1 Fibro	(ND)	14	167

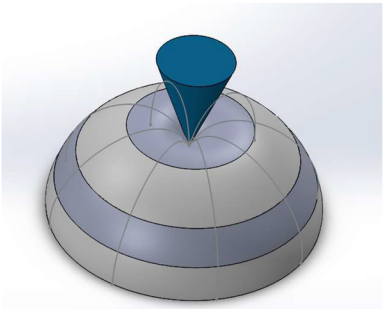

Conical indentor model

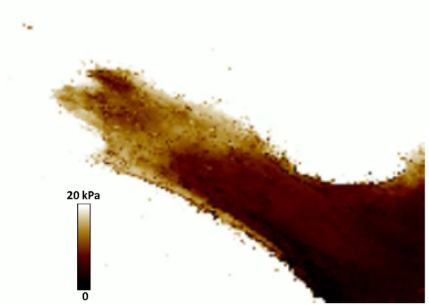

Young's modulus images

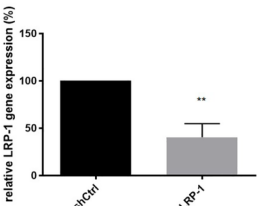

MDA-MB-231 & LRP-1 silencing

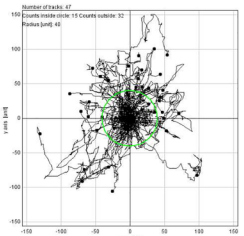

Migration